ACS OMEGA

Open Access

http://pubs.acs.org/journal/acsodf

Article

Development of a Low-Cost Paper-Based Platform for Coffee Ring-Assisted SERS

Anna S. Rourke-Funderburg, Alec B. Walter, Braden Carroll, Anita Mahadevan-Jansen, and Andrea K. Locke*

Cite This: *ACS Omega* 2023, 8, 33745−33754

Read Online

ACCESS | Metrics & More | Article Recommendations | Supporting Information

ABSTRACT: The need for highly sensitive, low-cost, and timely diagnostic technologies at the point of care is increasing. Surface-enhanced Raman spectroscopy (SERS) is a vibrational spectroscopic technique that is an advantageous technique to address this need, as it can rapidly detect analytes in small or dilute samples with improved sensitivity compared to conventional Raman spectroscopy. Despite the many advantages of SERS, one drawback of the technique is poor reproducibility due to variable interactions between nanoparticles and target analytes. To overcome this limitation, coupling SERS with the coffee ring effect has been implemented to concentrate and localize analyte−nanoparticle conjugates for improved signal reproducibility. However, current coffee ring platforms require laborious fabrication steps. Herein, we present a low-cost, two-step fabrication process for coffee ring-assisted SERS, utilizing wax-printed nitrocellulose paper. The platform was designed to produce a highly hydrophobic paper substrate that supports the coffee ring effect and tested using gold nanoparticles for SERS sensing. The nanoparticle concentration and solvent were varied to determine the effect of solution composition on ring formation and center clearance. The SERS signal was validated using 4-mercaptobenzoic acid (MBA) and tested with *Moraxella catarrhalis* bacteria to ensure functionality for chemical and biological applications. The limit of detection using MBA is 41.56 nM, and the biochemical components of the bacterial cell wall were enhanced with low spectral variability. The developed platform is advantageous due to ease of fabrication and use, representing the next step toward implementing low-cost coffee ring-assisted SERS for point-of-care sensing.

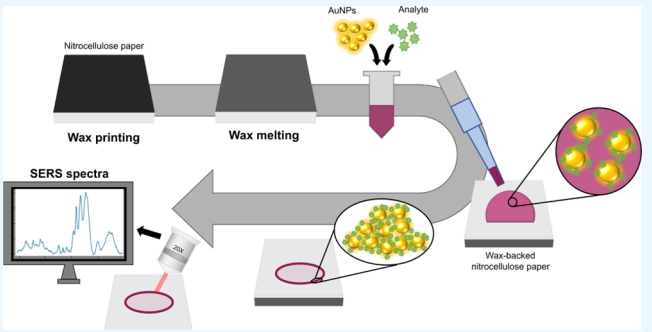

INTRODUCTION

With over 880 million doctor office visits in 2016 alone, and the sustained prevalence of infectious diseases, the need for faster and improved diagnostic technologies at the point of care is on the rise.[1,2] Microorganism culturing and polymerase chain reaction (PCR) are two of the most common diagnostic techniques, yet they have significant constraints. Both techniques have complex methodology and slow turnaround time for results due to multistep procedures. Recent advances in real-time diagnostics, such as real-time PCR, are still lacking due to significant limitations. Drawbacks such as a decrease in efficiency from standard PCR, the requirement for specific primer selections, and result dependency on sample handling and processing inhibit the widespread implementation of real-time PCR.[3−6] Thus, there is a lack of highly sensitive and specific, easy-to-use diagnostic technologies for point-of-care applications. Vibrational spectroscopy, specifically Raman spectroscopy, has gained popularity in addressing this need. Raman spectroscopy is a molecule-specific technique that provides a spectral fingerprint representative of the vibrational chemical bonds present in the sample. Using these spectral fingerprints, disease states and other medically relevant states can be determined.[7] Raman spectroscopy is a label-free, nondestructive method that can be used *in vivo* or *ex vivo* on collected tissue specimens or biofluids and can provide results in real time. Finally, this vibrational spectroscopic technique can be cost-effective and adapted for use in remote settings due to recent advancements in the reduction of instrumentation cost, improved sensitivity, and portability via handheld spectrometers.[8]

While Raman spectroscopy is a sensitive optical technique, the inherent weakness of the Raman scattering effect is a limitation hindering its widespread clinical implementation. To address this challenge, surface-enhanced Raman spectroscopy (SERS) positions analytes near metallic colloids or roughened metallic surfaces to produce spectral enhancements up to 10^{14} compared to conventional Raman scattering.[9,10] This analytical

Received: June 12, 2023
Accepted: July 14, 2023
Published: September 5, 2023

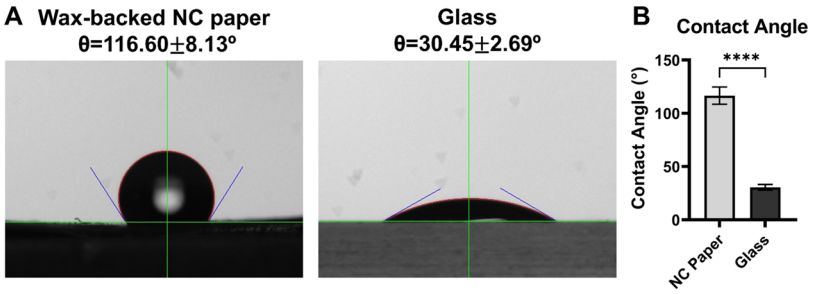

Figure 1. White light images showing the contact angle measurements for (A) the wax-backed nitrocellulose (NC) paper and standard glass slides; (B) the wax-backed NC paper has a significantly higher water contact angle indicating improved hydrophobicity (****$p < 0.0001$).

technique is highly specific, sensitive, and can enable single-molecule detection.[11] Numerous applications have been shown for SERS, including bacterial characterization and detection, detection of tumor cells and deleterious metabolic alterations, and detection of inflammatory molecules.[12−16] Additionally, SERS has gained popularity for nonbiological applications such as environmental pollutant screening and detection of inorganic molecules, ions, and toxic industrial chemicals.[10,17,18] While SERS shows substantial enhancement compared to conventional Raman spectroscopy, it has its own drawbacks. One of the most significant limitations of SERS is poor spectral reproducibility. This is caused by changes in the distance and interaction of analytes with the metallic substrates, which significantly alters the target and degree of enhancement.[19] As the interactions between the metallic substrates and analyte change, the enhancement changes and induces high variability in the SERS spectra.[20] Therefore, coupling of SERS with an analyte concentration technique, such as the coffee ring effect (CRE), can enhance reproducibility by regulating interactions between metallic substrates and analytes.[21] This coupling shows great promise for improving the reproducibility and usability of SERS in the clinical setting.

The CRE is a natural phenomenon where solutions spontaneously leave a ring on a surface upon drying. This results in solutes concentrated in a ring, while the center of the ring is left mostly empty. The main driving forces of the CRE are contact line pinning and evaporation.[22] Contact line pinning occurs when the outer edge of a droplet cannot move once dropped on a surface and can result from physical properties, such as roughness, or chemical properties, such as electrostatic interactions. These interactions between the fluid and surface immobilize the outer edge of the droplet, allowing for no further spread of the fluid. Evaporation of the droplet induces a radial capillary flow within the drying droplet and carries and deposits suspended particles to the contact line.[23] This capillary flow results from the liquid flowing from the center of the droplet to the edge to replace the fluid lost to evaporation, as the edge evaporates the quickest.[24] The natural concentrating and separating effect of the coffee ring is responsible for its widespread use in various scientific processes. It has been used for nanochromatography via separation of complex samples, screening environmental pollutants in river water, and detecting contaminants for food safety applications, among others.[21,23,25] It has also been utilized for biological applications such as identifying a malarial biomarker, detecting thrombin down to 2 ng/mL, and identifying point mutations in proteins based on protein adsorption and organization behavior in the resulting coffee ring.[26−28]

The combination of the CRE and SERS exploits the natural separating mechanism of the CRE to increase reproducibility of SERS, thus overcoming one of its most significant limitations. Previously in the literature, the combined platforms have been developed for applications such as detecting adulterants in milk, phenylalanine in urine, breast cancer cells in serum, and pharmaceuticals in urine.[21,29−31] However, these studies used nonideal substrates such as silicon wafers and glass. Achieving ideal coffee ring formation on these substrates can be time-consuming, with many applications necessitating vacuum drying chambers and/or heat sources to expedite this process. Extended drying times such as 12−24 h and drying temperatures up to 70 °C have been reported.[29,32,33] Further, some cases demand pretreated substrates for the ring effect to be observed, often requiring extensively treated glass slides or silica wafers, or patterned surfaces that physically restrict analyte flow to create the CRE.[34−37]

To the best of our knowledge, few paper-based coffee ring-SERS platforms exist yet lengthy fabrication processes are still needed to adequately achieve the CRE. These procedures include chemical hydrophobization, electrospinning, or colloidal nanoparticle soaking.[38−40] Additionally, poor center clearance is seen in previously reported paper-based substrates for coffee ring-SERS, which demonstrates a crucial drawback in the future application of these platforms.[40] The prolonged and complicated drying methods, complex substrate production, and incomplete analyte flow detract from the overall accessibility of the process but provide room for further improvements. Therefore, to simplify the substrate creation process and improve center clearance, we propose to use wax-printed nitrocellulose (NC) paper as an alternative paper-based substrate.

This work aims to create an easy-to-fabricate, low-cost paper-based SERS platform using hydrophobic wax and NC paper in a two-step process. The wax printing and melting are used to generate a hydrophobic substrate that sustains the CRE. Herein, we investigate the effect of modifying gold nanoparticles (AuNPs) concentration and solvent composition on the CRE. This platform was validated using 4-mercaptobenzoic acid (MBA) and *Moraxella catarrhalis* bacteria. To the best of our knowledge, this work also demonstrates the first utilization of paper-based coffee ring-SERS for bacterial characterization.

RESULTS AND DISCUSSION

The importance of a hydrophobic surface in the formation of the coffee rings has been well characterized in the literature and has been found to improve the concentrating effect of the

https://doi.org/10.1021/acsomega.3c03690
ACS Omega 2023, 8, 33745−33754

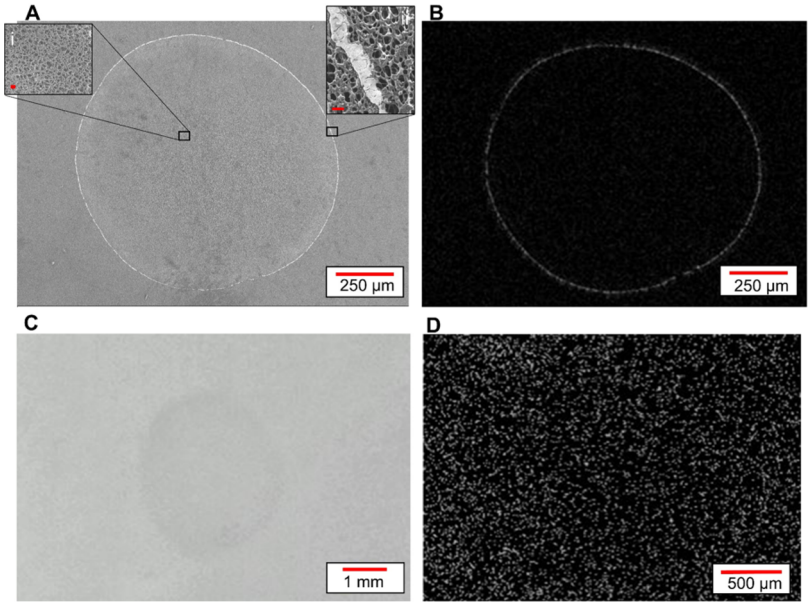

Figure 2. (A) SEM image of the coffee ring formed using AuNPs on the wax-backed paper substrate (135× magnification), inset i: center of coffee ring (5000× magnification, scale bar = 2 μm), inset ii: edge of coffee ring (12,000×, scale bar = 2 μm); (B) EDS map showing the location of elemental gold in the ring formed on the wax-backed paper (135× magnification); (C) white light image captured with a smartphone of faint ring formed without wax backing on paper; and (D) EDS map showing no localization of elemental gold when no-wax backing is used (95× magnification).

analyte, resulting in up to a 6-fold signal intensity increase from the ring.[26] In general, surfaces with a water contact angle of 90° or greater are classified as hydrophobic.[41] Therefore, other coffee ring-SERS substrates reported in the literature typically use multiple surface treatment to achieve hydrophobic surfaces with contact angles between 96 and 135°.[26,40,42] Herein, to generate a low-cost, easy-to-fabricate coffee ring platform, the printing and melting of wax on NC paper were explored. The resulting paper-based substrate has a hydrophobic surface with a water contact angle of 116.60 ± 8.13° (Figure 1A), which is comparable to the other reported coffee ring substrates but features a simple, two-step fabrication process. This platform is also significantly ($p < 0.0001$) more hydrophobic than a standard glass slide (30.45 ± 2.69°) as seen in Figure 1B. Thus, the paper-based substrate developed here is highly hydrophobic and reproducible. This hydrophobicity is due to the presence of the wax backing and subsequent wax melting. The melting of the wax partially through the paper creates a homogeneous coating of the inner and deeper fibers within the paper, resulting in confinement of liquids to the top surface and without radial flow. Additionally, this platform has a water contact angle in the range of other coffee ring-SERS platforms yet features a simplified fabrication process, which can aid in the widespread use of coffee ring-SERS.

Coffee Ring Characterization. To characterize the ring formation using AuNPs, scanning electron microscopy (SEM) and white light microscopy images of the coffee rings were obtained on NC paper with and without the wax present, respectively.

Figure 2A shows the SEM images of the coffee ring when the wax backing is present on the NC paper and reveals the localization of the AuNPs within a single ring (Figure 2A, inset). The localization of the AuNPs at the ring was confirmed using elemental analysis via energy-dispersive spectroscopy (EDS), which show elemental gold confined to a single ring with little to no gold in other areas of the paper (Figure 2B).

In comparison, when AuNPs were dropped on the bare NC paper with no wax backing, a much fainter ring is formed, indicating inadequate AuNPs flow and concentration at the droplet edge (Figure 2C). Upon further analysis of the location of elemental gold on the bare paper using EDS, the gold is not localized in any specific area and instead is distributed throughout the paper (Figure 2D). This further strengthens the importance of hydrophobic wax backing in the coffee ring formation process.

To confirm that contact lining pinning and the coffee ring mechanism were taking place, 0.5 μL of green food coloring solution was dropped on the wax-backed paper substrate and was imaged every minute throughout the drying process (Figure S1A). The droplet diameter was measured in two orientations (horizontal and vertical) on each image and averaged to create one diameter measurement for each timepoint. Each diameter was then plotted against the time to compare the droplet diameter across the total drying time (Figure S1B). Since top-view imaging was performed, for the first 1/3 of the drying process, the wider diameter of the droplet was imaged rather than the contact line. After approx. 1/3 of the drying time, the droplet collapses, and the diameter remains constant until fully dry and indicated no signs of radial flow. The stability of the droplet diameter confirms contact line pinning, thus confirming the drying mechanism via the CRE. This verifies that this simplistic platform supports the CRE and provides the added advantage of a 10 min drying time.

AuNPs Concentration Modulation. After confirming the successful formation of the coffee ring on the hydrophobic wax-backed NC paper, the effect of AuNPs concentration on ring formation and center clearance was investigated. A coffee ring formed under all AuNPs concentrations tested here (1.4, 7, 14 nM) (Figure 3A). Using RGB analysis, two metrics were utilized to quantify the formation of the ring: the clearance in the center of the ring and the concentration of particles at the ring. The ring intensity increased from 1.4 to 7 nM AuNPs

https://doi.org/10.1021/acsomega.3c03690
ACS Omega 2023, 8, 33745−33754

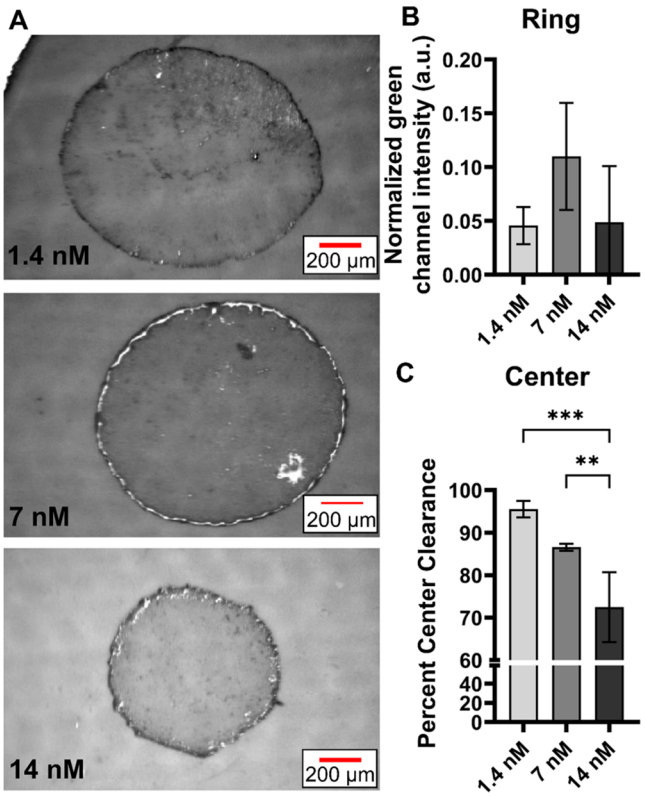

Figure 3. (A) Green channel images (5× magnification) of coffee rings formed using three different AuNPs concentrations; (B) no significant differences seen among the intensity at the rings for the different concentrations; and (C) center clearance of each ring shows a significantly decreased center clearance at the highest AuNPs concentration (14 nM) (**$p < 0.01$, ***$p < 0.001$).

concentration. However, no statistical difference was observed for the three concentrations at the ring (Figure 3B). This may be due to the presence of specular reflectance, evident in the images, affecting the RGB analysis. Regardlessly, at a 1.4 nM AuNPs concentration, the mean center clearance is 95.53%, demonstrating high clearance of the nanoparticles to form the coffee ring.

As AuNPs concentration increased, a significant decrease in center clearance was observed, yet at the highest AuNPs concentration, the mean center clearance remained above 70% (Figure 3C). This decrease in clearance could be partially due to the increased evaporation rate caused by increasing the AuNPs concentration. Nguyen et al. showed that as the concentration of particles increases, the evaporation of the droplet quickens.[43] Thus, not all nanoparticles can travel to the outer ring before the droplet fully evaporates, and they are deposited in the center, decreasing the center clearance. These nanoparticles deposited in the center rather than on the ring could reduce the SERS signal and limit the usability of coffee ring-assisted SERS for analyte detection, especially at low concentrations. Therefore, using a lower concentration of the citrate-capped nanoparticles in water is advantageous as it could yield a strong SERS signal due to its high center clearance and confinement of the particles to a singular continuous ring.

Effect of Surfactant on Coffee Ring Formation. Surfactants, such as Tween-20, are commonly used in assays to prevent nonspecific binding. However, when used in a coffee ring application, Tween can suppress the CRE due to significant changes to the surface tension in an evaporating droplet.[44,45] To study this in a paper-based coffee ring, the 1.4 and 7 nM AuNPs concentrations were used to determine the influence of Tween at varying concentrations (0.0005−2% (v/v)). Visually, at higher concentrations of Tween [>0.001%], the coffee rings were seen to be discontinuous, which is believed to be due to micelle formation (Figure 4C).[46−49] At Tween concentrations of 0.001% and lower, there was no visible disruption in the rings. Moreover, the presence of Tween at these lower concentrations significantly improved the center clearance of the AuNPs on the paper (Figure 4A,B). At both 1.4 and 7 nM AuNPs concentrations, increasing concentrations of Tween up to 0.001% increased the center clearance from 95.53 to 98.78 and 86.56 to 92.13%, respectively. We hypothesize that the Tween reduces any nonspecific binding interactions present, which further improves the clearance.[50] Furthermore, the presence of Tween shows a minimum effect on the ring intensities of either AuNPs concentration in comparison to the results obtained using no surfactant (Figure S2). Therefore, while Tween has previously been shown in the literature to disrupt the CRE, concentrations at or below 0.001% showed to improve nanoparticle flow without disrupting ring formation; thus, this platform can be utilized in applications necessitating Tween.

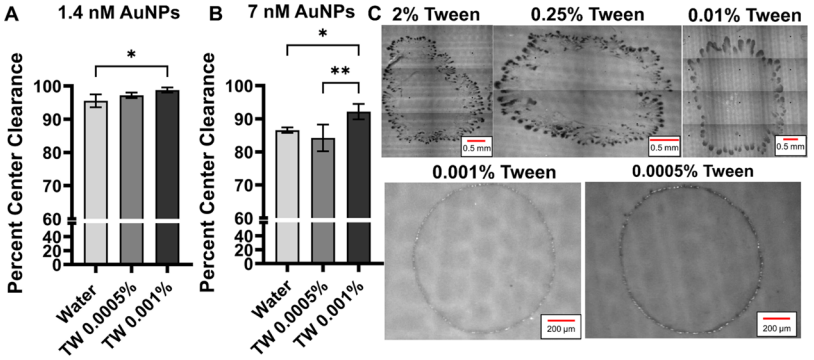

Figure 4. Comparison of center clearance using varying concentrations of Tween-20 for 1.4 and 7 nM AuNPs concentrations: (A) trend of increasing center clearance with the addition of Tween for the 1.4 nM AuNPs concentration; (B) percent center clearance of the ring is significantly higher when using Tween 0.001% as compared to water for the 7 nM AuNPs concentration; and (C) green channel images (5× magnification) showing the effect of varying the surfactant concentration (*$p < 0.05$, **$p < 0.01$).

https://doi.org/10.1021/acsomega.3c03690
ACS Omega 2023, 8, 33745−33754

SERS Characterization Using MBA. To investigate SERS signal intensity and the location of enhancement in the coffee ring on the developed NC paper-based platform, we utilized MBA, a common Raman reporter molecule, to generate SERS maps and point measurements across the rings. First, to validate that the coffee ring formation significantly improved the SERS signal, Figure 5 shows a 20-fold signal increase when utilizing the wax-backed NC paper compared to the NC paper with no wax backing.

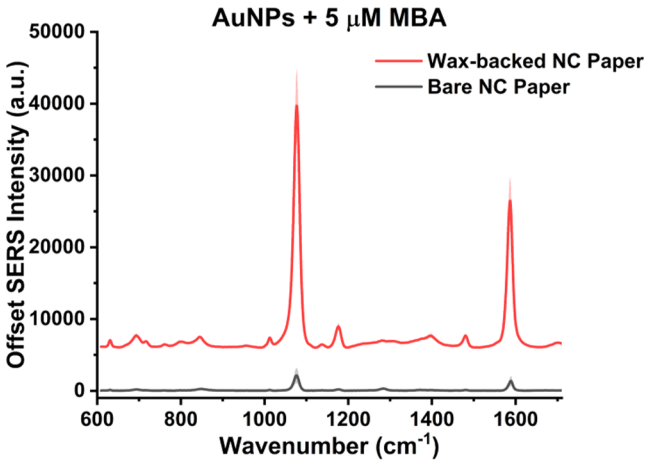

Figure 5. SERS spectra of 5 μM MBA with 0.7 nM AuNPs on the wax-backed paper substrate (red) and on NC paper with no wax backing (gray) (shaded error bars = standard deviation).

Second, a SERS map was generated for a coffee ring formed using only AuNPs to establish a baseline in the absence of MBA. Cluster analysis with hierarchical cluster analysis (HCA) revealed nonspecific enhancement of the NC paper, represented in cluster 2, particularly in the 1200−1400 and 1600−1700 cm^{-1} regions, and the unenhanced NC paper spectra represented in cluster 1 (Figure 6A). However, this enhancement shows minimal SERS signal (<1000 a.u.) and is not evident at high concentrations of MBA (Figure 6B). SERS maps were repeated for a coffee ring formed from a solution of 5 μM MBA with 0.7 nM AuNPs on the wax-backed paper.

A gradient was identified based on well-known peaks of 4-MBA at 1076 and 1586 cm^{-1}.[51] After analysis with HCA, the average spectra of each cluster were calculated and plotted (Figure 6B). HCA analysis shows that this gradient is formed with the highest intensity MBA signal in the dark red region (cluster 4, Figure 6B) and two lower regions of MBA signal (clusters 2 and 3, Figure 6B). The lower intensity MBA signal at cluster 2 present at the center may be due to residual nanoparticles since ∼95% center clearance was noted previously (Figure 4A). To investigate the repeatability of SERS measurements using this platform, five spectra were taken at different points along the AuNPs ring and were plotted separately. These measurements resulted in a mean and standard deviation of the 1076 cm^{-1} peak of 3485.92 ± 349.71, showing the repeatability of the SERS signal (Figure S3).

Limit of Detection. Next, the limit of detection (LOD) was determined via point spectra obtained from the mixture of various concentrations of MBA (0−5 μM) with fixed AuNPs concentration on triplicate paper-based platforms (Figure 6C). The SERS intensity at 1076 cm^{-1} peak, representative of

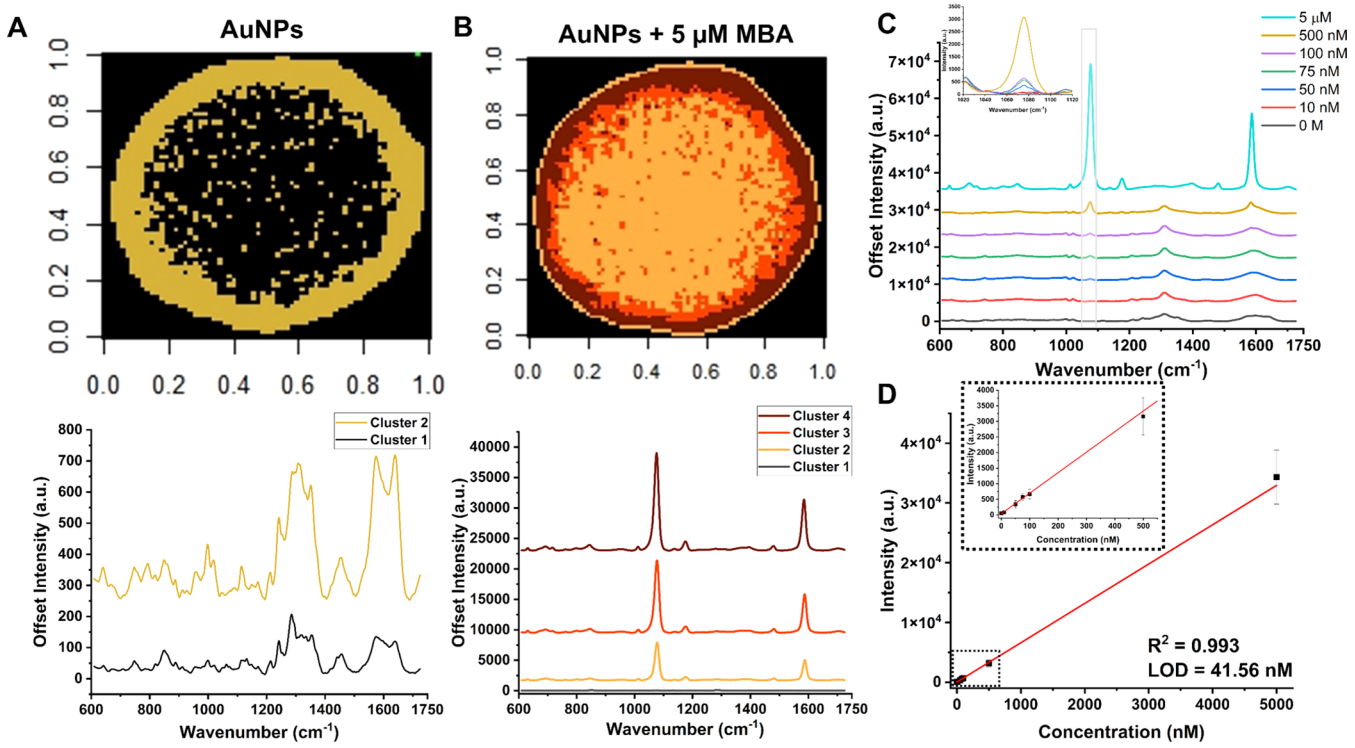

Figure 6. (A,B) SERS maps using (A) 0.7 nM AuNPs and (B) 0.7 nM AuNPs + 5 μM MBA; (C) stacked spectra of MBA mixed with AuNPs highlighting the MBA peak at 1076 cm^{-1} peak (gray box), with the inset showing 1020−1120 cm^{-1} plotted for the MBA concentrations of 0−500 nM; and (D) scatter plot with the inset highlighting lower concentrations (10−500 nM MBA) with limit of detection (LOD) and goodness of fit reported.

https://doi.org/10.1021/acsomega.3c03690
ACS Omega 2023, 8, 33745−33754

benzene ring breathing modes, was plotted against the MBA concentration (Figure 6D). The linear working range of the wax-backed paper platform was determined to be 50 nM to 5 μM with an LOD of 4.156 × 10^{-8} M (Figure 6D). This LOD is similar to those found in the literature for various other paper-based coffee ring-SERS platforms (10^{-8} to 10^{-9} M) and is within the range of LODs cited for non-paper-based coffee ring-SERS substrates (10^{-6} to 10^{-12} M).[29,36,39]

SERS of Bacteria Using Coffee Ring Effect. To demonstrate the applicability of the paper-based platform for biological samples, *M. catarrhalis* was introduced to the coffee ring substrate. The mixture of *M. catarrhalis* and AuNPs produced a ring, with increasing gradient (Figure 7A).

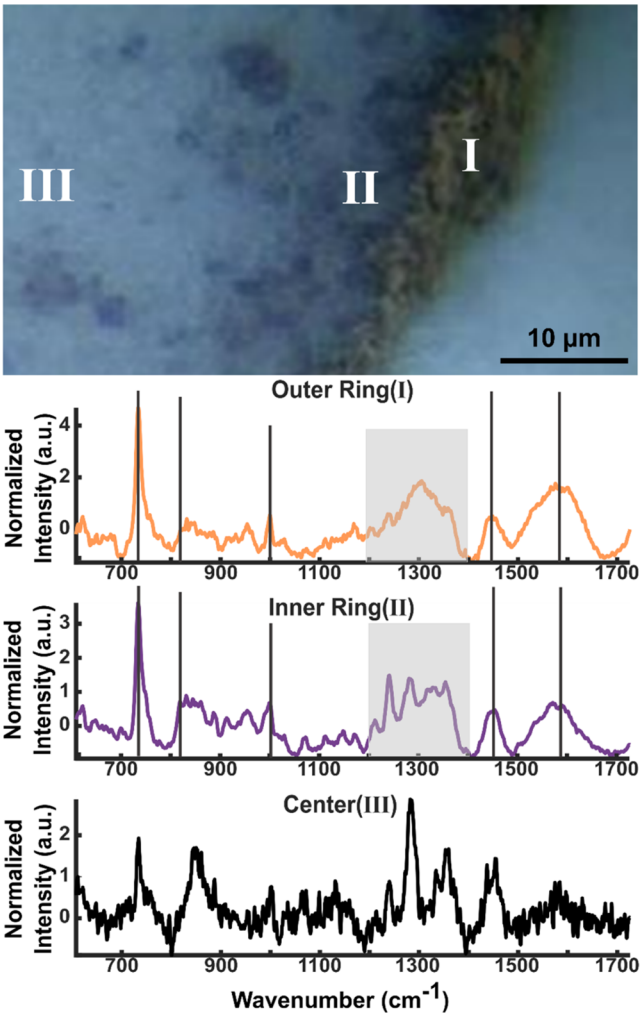

Figure 7. *M. catarrhalis* on the paper substrate formed three regions (I: outer ring, II: inner gradient of the outer ring, III: cleared ring center): white light microscopy image (100× magnification) and averaged spectra for each of the regions, black lines show bacterial peaks of interest and gray box shows the area of the spectra that was excluded in peak identification due to paper background.

Distinct bacterial spectral features are observed in both the inner (region II) and outer portions of the ring (region I). The most prominent peaks identified in the spectra include the 732 cm^{-1} peak known to be from adenine in the cell wall, the 1000 cm^{-1} phenylalanine peak, and the 1450 cm^{-1} peak indicating protein-based structures (Table S1).[9,52−55]

The peaks represent cell wall components due to the location dependency of SERS in which only molecules within 2−10 nm of nanoparticles are enhanced.[56] These spectral features correlate with prior publications on SERS of bacteria; agreeance is also seen in publications detailing the SERS spectra of Gram-negative bacteria, further reinforcing that the *M. catarrhalis* is being enhanced.[57] The center of the ring shows a sharp peak at approximately 1280 cm^{-1} due to the enhancement of the paper. However, minimal bacterial spectral features were observed in the center, confirming that the coffee ring platform was capable of concentrating the bacteria within the ring.

To assess reproducibility, spectra collected from three separate samples (five spectra per ring) were plotted with shaded error bars (mean ± SD) (Figure S4). The mean and standard deviation for the 732 cm^{-1} peak were calculated for the inner portion and outer portion of the ring to be 4.30 ± 1.64 (inner) and 4.83 ± 1.47 (outer), respectively, showing reproducibility. Further, the bacterial concentration utilized herein (~7.3 × 10^4 CFU/mL) is similar to the concentration used by other works detailing SERS of bacteria (10^2−10^9 CFU/mL), highlighting the potential biological application of this platform.[58−60]

CONCLUSIONS

Herein, a novel platform for coffee ring-enhanced SERS was developed using commercially available NC paper and wax printing. This paper-based platform is advantageous over previously reported coffee ring-SERS substrates in its simplified fabrication, ring drying time, and biological utility. Previous substrates report complex fabrication, including a 5-step washing and chemical treatment protocol, expensive substrates such as quartz, or the use of potentially hazardous materials. The platform proposed in this work decreases the fabrication protocol to two steps, wax printing and melting, utilizes commonly available NC paper, and does not require any hazardous chemicals for production. Furthermore, the developed platform poses a more beneficial drying process that does not require an oven, a vacuum chamber, or a lengthy drying time as reported by other methods. In addition to the simplified fabrication process, this paper-based platform shows comparable analyte localization and enhancement capabilities to those reported in the literature for both chemical and biological samples. To the best of our knowledge, this study is also the first to demonstrate the use of paper-based coffee ring-SERS for bacterial characterization. Future works look at optimizing methods to reduce the background noise from the paper and will further optimize the platform for dilute biological applications. Overall, this paper substrate shows great promise for the next step in the broad implementation of coffee ring-assisted SERS for point-of-care diagnostics.

METHODS

Materials. NC membranes with a pore size of 0.45 μm and brain heart infusion (BHI) media were purchased from Fisher Scientific (Hampton, NH). Gold (III) chloride hydrate ($HAuCl_4$), nitric acid (HNO_3), hydrochloric acid (HCl), agar, trisodium citrate ($Na_3C_6H_5O_7$), 4-mercaptobenzoic acid (MBA), and Tween-20 (polysorbate 20) were purchased from Sigma-Aldrich (St. Louis, MO). Wax ink was purchased from Xerox (Norwalk, CT). *Moraxella catarrhalis* (*M. catarrhalis*, strain AmMS 116, ATCC #49143) was purchased from

https://doi.org/10.1021/acsomega.3c03690
ACS Omega 2023, 8, 33745−33754

American Type Culture Collection (ATCC) (Manassas, VA). All chemicals were of analytical grade and used with no additional purification.

Hydrophobic Nitrocellulose Paper Substrate. The hydrophobic wax-backed paper substrate was created using the standard NC blotting membrane paper (pore size 0.45 μm, GE Healthcare Amersham, Chicago, IL) and a wax printer (ColorQube 8570, Xerox; Norwalk, CT). One side of the NC paper was printed with black wax ink and then melted at 150 °C for 1 min to allow the wax to advance through the paper without complete protrusion on the other side (Figure S5). The hydrophobicity of the wax-backed substrate was verified by measuring the water contact angle (Model 200-F4 Contact Angle Goniometer and DROPimage Advanced Software v.2.6.1; ramé-hart, Succasunna, NJ) 5 times to verify reproducibility. As a comparison to the substrate's hydrophobicity, the water contact angle of glass was measured five times since glass is one of the most common substrates for coffee ring applications.

Coffee Ring Characterization. AuNPs (25 nm, 1.4 nM; Figure S6) were synthesized as described in the Supplementary Information. The coffee rings were obtained by applying a 1 μL droplet of AuNPs to the wax-backed substrate and allowed to dry at 25 °C until completely dry, which took approximately 10 minutes. A 1 μL droplet of AuNPs was applied to the NC paper with no-wax backing to compare the effect of the hydrophobic coating and was imaged using a smartphone (OnePlus, OnePlus Technology, Shenzhen, Guangdong). Scanning electron microscopy (SEM) (Merlin scanning electron microscope, Carl Zeiss; Germany) was utilized to visualize the dried coffee rings, and energy-dispersive X-ray spectroscopy (EDS) (Xmax 50 Silicon Drift Detector EDS, Oxford Instruments; United Kingdom) was performed to examine the location of elemental gold, ensuring the nanoparticles traveled to the edge of the ring. Finally, to confirm the coffee ring mechanism, a 0.5 μL droplet of green food coloring (25 μL food coloring:1 mL DI water) was dropped on the wax-backed NC paper and imaged every 1 minute using white light microscopy (Leica microscope, Leica Microsystems; Germany) at a 5× magnification (NA = 0.12) until fully dried. The diameter of the droplet in each image was measured using ImageJ (imagej.nih.gov).

Nanoparticle Concentration and Solvent Modulation. Following the coffee ring characterization, the influence of solution composition was investigated by modulating the AuNPs concentration and introducing a surfactant, Tween-20. First, nanoparticle concentrations of 1.4, 7, and 14 nM were used (1×, 5×, and 10× respectively). A 1 μL droplet of each concentration was applied to the substrate and allowed to dry; each condition was repeated five times. After drying, an image of each formed ring was taken using white light microscopy (5× magnification) for RGB analysis via ImageJ. The effect of the surfactant on ring formation was studied using varying concentrations of Tween-20 in DI water for the 1.4 and 7 nM AuNPs concentrations. The Tween-20 concentration was varied between 0.0005 and 2% (v/v). The AuNPs were centrifuged at 3300g for 5 min, and the supernatant was removed and replaced with an equal volume of Tween-20 solutions. Again, 1 μL was dropped on the coffee ring paper substrate and allowed to dry fully. After drying, an image was taken in the same manner as above.

RGB Analysis. Each image was imported into ImageJ as a JPEG file to undergo RGB analysis.[61] Six regions of interest (ROIs) were selected in each image: four background ROIs of the area outside the ring, one ROI of the entire ring, and one ROI of the inside of the ring following previously published methods[28] (Figure S7). The green channel was chosen for analysis since the absorbance of the AuNPs is in the green region of the electromagnetic spectrum. The mean of each background ROIs was averaged together to quantify the background intensity for each sample. The center clearance of the ring, indicating how well the nanoparticles traveled toward the ring, was quantified using percent center clearance. This percent center clearance was calculated by normalizing the average intensity from the inner ROI by the average background intensity eq 1. To quantify the ring intensity, the absolute value of the average inner and average full ring ROI was normalized to the average background intensity, and the difference was taken eq 2

$$\text{center clearance} = \frac{\text{inner ROI intensity}}{\text{avg background intensity}} \quad (1)$$

$$\text{ring intensity} = \frac{\text{full ROI intensity}}{\text{avg background intensity}} - \frac{\text{inner ROI intensity}}{\text{avg background intensity}} \quad (2)$$

SERS Characterization. After investigating the effect of changing solution parameters, the SERS enhancement and LOD of the substrate were determined using MBA. AuNPs and MBA were mixed at a 1:1 volumetric ratio for a final AuNPs concentration of 0.7 nM and MBA concentration ranging from 10 nM to 5 μM. A 1 μL droplet of this solution was applied to the substrate and allowed to dry fully; each condition was repeated in triplicate. Additionally, a 1 μL droplet of the 5 μM MBA + AuNPs solution was dropped on the NC paper with no wax backing to investigate the effect of the coffee ring formation on the SERS enhancement. This was also repeated in triplicate. Subsequently, SERS measurements were collected using a benchtop Raman microscope (Renishaw inVia confocal Raman microscope, Renishaw; United Kingdom) equipped with a 785 nm laser diode in combination with a thermoelectrically cooled charged-coupled device (CCD) camera and a grating of 1200 l/mm. Multiple point spectra (5 per sample) were collected under 20× magnification (NA = 0.4) with 2.16 mW of power and a total integration time of 10 s. Spectra were taken from the edge of the ring and were averaged to obtain one spectrum per sample. SERS maps were also collected by point scanning at a 15 μm step size over the entire area of the coffee ring using the same power as the point measurements with a 2 s total integration time. After collection, spectra and maps were processed with a 2nd order Savitzky−Golay filter for noise smoothing and asymmetric least-squares regression (ALSR) for background fluorescence subtraction.[62,63] Maps were then analyzed by principal component analysis (PCA) for dimension reduction followed by hierarchical cluster analysis (HCA) to separate and visualize the SERS signal generated by MBA and the substrate's background.[64] This was then plotted against the map coordinates for each point, generating a color map of the SERS signal from the coffee ring. The LOD was analyzed by plotting the intensity of the 1076 cm^{-1} peak for each MBA concentration and performing a linear fit.

***M. catarrhalis* SERS.** The enhancement of a common bacteria was investigated to demonstrate the utility of the

https://doi.org/10.1021/acsomega.3c03690
ACS Omega 2023, 8, 33745−33754

developed coffee ring-SERS platform for biological applications. *M. catarrhalis* was cultured from a frozen stock on BHI agar plates at 37 °C under 5% CO_2 for 24 h. A liquid culture was grown by transferring a single colony to 10 mL of BHI broth and was allowed to incubate for 24 h (37 °C and 5% CO_2). The cultures were then washed with DI water twice using centrifugation at 3300*g* for 8 min, and 1 mL of washed culture was collected for optical density (OD) readings at 600 nm to quantify the bacterial concentration using an ultraviolet−visible−near-infrared (UV−vis−NIR) spectrophotometer (Agilent Technologies; Santa Clara, California). After determining the OD, the bacteria were resuspended with Tween 0.0005% in DI water. Washed liquid cultures (OD = 0.45, ~7.3×10^4 CFU/mL) and AuNPs (14 nM) were mixed using a 1:4 volumetric ratio by pipetting. A 1 μL drop of the solution was applied to the substrate and allowed to dry. Five SERS spectra were taken using the Raman microscope from three regions of the dried coffee ring: the center of the ring, the outer edge of the ring, and inside the outer ring. Spectra were taken under a 100× magnification (NA = 0.85) with a power of 0.2 mW at the sample with a total of a 5 s integration time. At each of the three locations, the five SERS spectra were averaged to obtain one spectrum per location per sample. The experiments were conducted in triplicate. Spectra were processed by smoothing and fluorescence subtraction, as stated previously, and normalized using standard normal variate (SNV).

Statistical Analysis. The contact angle of the coffee ring substrate and standard glass was compared using an unpaired *t*-test. The AuNPs concentration RGB values and influence of Tween-20 concentration were analyzed using ordinary one-way ANOVAs and Tukey's multiple comparison tests.[65] An α value of 0.05 was used for all statistical analyses. Statistical analysis was performed using GraphPad Prism 9 (GraphPad Software; San Diego, CA), and HCA analysis was performed in R in RStudio (RStudio; Boston, MA). Curve fitting to determine LOD was performed in Origin (OriginLab, Northampton, MA). Raman processing was performed in MATLAB (MathWorks; Natick, MA). All data are presented as mean ± standard deviation, except where otherwise indicated.

■ ASSOCIATED CONTENT

Supporting Information

The Supporting Information is available free of charge at https://pubs.acs.org/doi/10.1021/acsomega.3c03690.

AuNPs synthesis methods; images of paper substrate fabrication; AuNPs absorbance spectra; ROI procedure; white light images of droplet drying and droplet diameter through drying; intensity of the ring at each surfactant concentrations; 5 spectra taken from coffee ring; *M. catarrhalis* replicates plotted as shaded error bars; and *M. catarrhalis* bacterial Raman peaks of interest (PDF)

■ AUTHOR INFORMATION

Corresponding Author

Andrea K. Locke − *Department of Biomedical Engineering, Vanderbilt University, Nashville, Tennessee 37240-0002, United States; Vanderbilt Biophotonics Center and Department of Chemistry, Vanderbilt University, Nashville, Tennessee 37240-0002, United States;* orcid.org/0000-0002-7357-9688; Email: andrea.locke@vanderbilt.edu

Authors

Anna S. Rourke-Funderburg − *Department of Biomedical Engineering, Vanderbilt University, Nashville, Tennessee 37240-0002, United States; Vanderbilt Biophotonics Center, Vanderbilt University, Nashville, Tennessee 37240-0002, United States;* orcid.org/0000-0002-7043-1370

Alec B. Walter − *Department of Biomedical Engineering, Vanderbilt University, Nashville, Tennessee 37240-0002, United States; Vanderbilt Biophotonics Center, Vanderbilt University, Nashville, Tennessee 37240-0002, United States*

Braden Carroll − *Vanderbilt Biophotonics Center, Vanderbilt University, Nashville, Tennessee 37240-0002, United States*

Anita Mahadevan-Jansen − *Department of Biomedical Engineering, Vanderbilt University, Nashville, Tennessee 37240-0002, United States; Vanderbilt Biophotonics Center, Vanderbilt University, Nashville, Tennessee 37240-0002, United States*

Complete contact information is available at: https://pubs.acs.org/10.1021/acsomega.3c03690

Notes

The authors declare no competing financial interest.

■ ACKNOWLEDGMENTS

This work was supported by the Vanderbilt Academic Pathways Fellowship Program (A.K.L) and the Vanderbilt Institute of Nanoscale Science and Engineering pilot funding (A.M.J). Finally, the authors would like to thank Dr. Rekha Gautam for her assistance with HCA data analysis.

■ REFERENCES

(1) FastStats - Physician office visits, 2021. https://www.cdc.gov/nchs/fastats/physician-visits.htm (accessed August 05, 2021).

(2) Center for Health Statistics, N. *Selected Nationally Notifiable Disease Rates and Number of New Cases: United States, Selected Years 1950-2018, United States : Table 10*, Hyattsville, MD; 2019, (accessed August 04, 2021).

(3) Sebastian, D.; Sebastian, D. Principles of Diagnosis. In *Principles of Manual Therapy (A Manual Therapy Approach to Musculoskeletal Dysfunction)*; Jaypee Brothers Medical Publishers (P) Ltd., 2005, Chapter 10.

(4) Bustin, S. A. How to Speed up the Polymerase Chain Reaction. *Biomol. Detect. Quantif.* **2017**, *12*, 10−14.

(5) Singh, J.; Birbian, N.; Sinha, S.; Goswami, A. A Critical Review on PCR, Its Types and Applications. *Int. J. Adv. Res. Biol.Sci* **2014**, *1*, 65−80.

(6) Kuang, J.; Yan, X.; Genders, A. J.; Granata, C.; Bishop, D. J. An Overview of Technical Considerations When Using Quantitative Real-Time PCR Analysis of Gene Expression in Human Exercise Research. *PLoS One* **2018**, *13*, No. e0196438.

(7) Lasch, P.; Kneipp, J. *Biomedical Vibrational Spectroscopy*; John Wiley & Sons, 2008.

(8) das Chagas e Silva de Carvalho, L. F.; Nogueira, M. S. Optical Techniques for Fast Screening − Towards Prevention of the Coronavirus COVID-19 Outbreak. *Photodiagn. Photodyn. Ther.* **2020**, *30*, No. 101765.

(9) Movasaghi, Z.; Rehman, S.; Rehman, I. U. Raman Spectroscopy of Biological Tissues. *Appl. Spectrosc. Rev.* **2007**, *42*, 493−541.

(10) Sharma, B.; Frontiera, R. R.; Henry, A. I.; Ringe, E.; Van Duyne, R. P. SERS: Materials, Applications, and the Future. *Mater. Today* **2012**, *15*, 16−25.

(11) Liu, Y.; Zhou, H.; Hu, Z.; Yu, G.; Yang, D.; Zhao, J. Label and Label-Free Based Surface-Enhanced Raman Scattering for Pathogen Bacteria Detection: A Review. *Biosens. Bioelectron.* **2017**, *94*, 131−140.
(12) Premasiri, W. R.; Moir, D. T.; Klempner, M. S.; Krieger, N.; G, J. I.; Ziegler, L. D. Characterization of the Surface Enhanced Raman Scattering (SERS) of Bacteria. *J. Phys. Chem. B* **2005**, *109*, 312−320.
(13) Kearns, H.; Goodacre, R.; Jamieson, L. E.; Graham, D.; Faulds, K. SERS Detection of Multiple Antimicrobial-Resistant Pathogens Using Nanosensors. *Anal. Chem.* **2017**, *89*, 12666−12673.
(14) Plou, J.; García, I.; Charconnet, M.; Astobiza, I.; García-Astrain, C.; Matricardi, C.; Mihi, A.; Carracedo, A.; Liz-Marzán, L. M. Multiplex SERS Detection of Metabolic Alterations in Tumor Extracellular Media. *Adv. Funct. Mater.* **2020**, *30*, No. 1910335.
(15) Yi, N.; Zhang, C.; Song, Q.; Xiao, S. A Hybrid System with Highly Enhanced Graphene SERS for Rapid and Tag-Free Tumor Cells Detection. *Sci. Rep.* **2016**, *6*, No. 25134.
(16) Li, D.; Jiang, L.; Piper, J. A.; Maksymov, I. S.; Greentree, A. D.; Wang, E.; Wang, Y. Sensitive and Multiplexed SERS Nanotags for the Detection of Cytokines Secreted by Lymphoma. *ACS Sens.* **2019**, *4*, 2507−2514.
(17) Cong, S.; Wang, Z.; Gong, W.; Chen, Z.; Lu, W.; Lombardi, J. R.; Zhao, Z. Electrochromic Semiconductors as Colorimetric SERS Substrates with High Reproducibility and Renewability. *Nat. Commun.* **2019**, *10*, No. 678.
(18) Alvarez-Puebla, R. A.; dos Santos, D. S., Jr.; Aroca, R. F. SERS Detection of Environmental Pollutants in Humic Acid− Gold Nanoparticle Composite Materials. *Analyst* **2007**, *132*, 1210−1214.
(19) Kim, N.; Thomas, M. R.; Bergholt, M. S.; Pence, I. J.; Seong, H.; Charchar, P.; Todorova, N.; Nagelkerke, A.; Belessiotis-Richards, A.; Payne, D. J.; Gelmi, A.; Yarovsky, I.; Stevens, M. M. Surface Enhanced Raman Scattering Artificial Nose for High Dimensionality Fingerprinting. *Nat. Commun.* **2020**, *11*, No. 207.
(20) Langer, J.; de Aberasturi, D. J.; Aizpurua, J.; Alvarez-Puebla, R. A.; Auguié, B.; Baumberg, J. J.; Bazan, G. C.; Bell, S. E. J.; Boisen, A.; Brolo, A. G.; Choo, J.; Cialla-May, D.; Deckert, V.; Fabris, L.; Faulds, K.; de Abajo, F. J. G.; Goodacre, R.; Graham, D.; Haes, A. J.; Haynes, C. L.; Huck, C.; Itoh, T.; Käll, M.; Kneipp, J.; Kotov, N. A.; Kuang, H.; Le Ru, E. C.; Lee, H. K.; Li, J. F.; Ling, X. Y.; Maier, S. A.; Mayerhöfer, T.; Moskovits, M.; Murakoshi, K.; Nam, J. M.; Nie, S.; Ozaki, Y.; Pastoriza-Santos, I.; Perez-Juste, J.; Popp, J.; Pucci, A.; Reich, S.; Ren, B.; Schatz, G. C.; Shegai, T.; Schlücker, S.; Tay, L. L.; Thomas, K. G.; Tian, Z. Q.; van Duyne, R. P.; Vo-Dinh, T.; Wang, Y.; Willets, K. A.; Xu, C.; Xu, H.; Xu, Y.; Yamamoto, Y. S.; Zhao, B.; Liz-Marzán, L. M. Present and Future of Surface-Enhanced Raman Scattering. *ACS Nano* **2020**, *14*, 28−117.
(21) Hussain, A.; Sun, D.-W.; Pu, H. SERS Detection of Urea and Ammonium Sulfate Adulterants in Milk with Coffee Ring Effect. *Food Addit. Contam.: Part A* **2019**, *36*, 851−862.
(22) Mampallil, D.; Eral, H. B. A Review on Suppression and Utilization of the Coffee-Ring Effect. *Adv. Colloid Interface Sci.* **2018**, *252*, 38−54.
(23) Wong, T. S.; Chen, T. H.; Shen, X.; Ho, C. M. Nano-chromatography Driven by the Coffee Ring Effect. *Anal. Chem.* **2011**, *83*, 1871−1873.
(24) Deegan, R. D.; Bakajin, O.; Dupont, T. F.; Huber, G.; Nagel, S. R.; Witten, T. A. Capillary Flow as the Cause of Ring Stains from Dried Liquid Drops. *Nature* **1997**, *389*, 827−829.
(25) Xu, J.; Du, J.; Jing, C.; Zhang, Y.; Cui, J. Facile Detection of Polycyclic Aromatic Hydrocarbons by a Surface-Enhanced Raman Scattering Sensor Based on the Au Coffee Ring Effect. *ACS Appl. Mater. Interfaces* **2014**, *6*, 6891−6897.
(26) Wen, J. T.; Ho, C. M.; Lillehoj, P. B. Coffee Ring Aptasensor for Rapid Protein Detection. *Langmuir* **2013**, *29*, 8440−8446.
(27) Devineau, S.; Anyfantakis, M.; Marichal, L.; Kiger, L.; Morel, M.; Rudiuk, S.; Baigl, D. Protein Adsorption and Reorganization on Nanoparticles Probed by the Coffee-Ring Effect: Application to Single Point Mutation Detection. *J. Am. Chem. Soc.* **2016**, *138*, 11623−11632.
(28) Gulka, C. P.; Swartz, J. D.; Trantum, J. R.; Davis, K. M.; Peak, C. M.; Denton, A. J.; Haselton, F. R.; Wright, D. W. Coffee Rings as Low-Resource Diagnostics: Detection of the Malaria Biomarker Plasmodium Falciparum Histidine-Rich Protein-II Using a Surface-Coupled Ring of Ni(II)NTA Gold-Plated Polystyrene Particles. *ACS Appl. Mater. Interfaces* **2014**, *6*, 6257−6263.
(29) Murugesan, B.; Yang, J. Tunable Coffee Ring Formation on Polycarbonate Nanofiber Film for Sensitive SERS Detection of Phenylalanine in Urine. *ACS Omega* **2019**, *4*, 14928−14936.
(30) Lin, X.; Jia, X.; Lin, J. Y.; Wu, P. H.; Weng, Y.; Feng, S. A Comparative Study Based on Serum SERS Spectra in and on the Coffee Ring for High Precision Breast Cancer Detection. *J. Raman Spectrosc.* **2022**, *53*, 1371−1379.
(31) Zhu, Q.; Yu, X.; Wu, Z.; Lu, F.; Yuan, Y. Antipsychotic Drug Poisoning Monitoring of Clozapine in Urine by Using Coffee Ring Effect Based Surface-Enhanced Raman Spectroscopy. *Anal. Chim. Acta* **2018**, *1014*, 64−70.
(32) Cao, R.; Pan, Z.; Tang, H.; Wu, J.; Tian, J.; Nilghaz, A.; Li, M. Understanding the Coffee-Ring Effect of Red Blood Cells for Engineering Paper-Based Blood Analysis Devices. *Chem. Eng. J.* **2020**, *391*, No. 123522.
(33) Hong, Y.; Li, Y.; Huang, L.; He, W.; Wang, S.; Wang, C.; Zhou, G.; Chen, Y.; Zhou, X.; Huang, Y.; Huang, W.; Gong, T.; Zhou, Z. Label-Free Diagnosis for Colorectal Cancer through Coffee Ring-Assisted Surface-Enhanced Raman Spectroscopy on Blood Serum. *J Biophotonics* **2020**, *13*, No. e201960176.
(34) Xu, J.; Du, J.; Jing, C.; Zhang, Y.; Cui, J. Facile Detection of Polycyclic Aromatic Hydrocarbons by a Surface-Enhanced Raman Scattering Sensor Based on the Au Coffee Ring Effect. *ACS Appl. Mater. Interfaces* **2014**, *6*, 6891−6897.
(35) Wang, W.; Yongguang, Y.; Zhiqiang, T.; Jingfu, L. Coffee-Ring Effect-Based Simultaneous SERS Substrate Fabrication and Analyte Enrichment for Trace Analysis. *Nanoscale* **2014**, *6*, 9588−9593.
(36) Juneja, S.; Bhattacharya, J. Coffee Ring Effect Assisted Improved S. Aureus Screening on a Physically Restrained Gold Nanoflower Enriched SERS Substrate. *Colloids Surf., B* **2019**, *182*, No. 110349.
(37) Zhang, J.; Zhang, Y.; Shi, G. Interface Engineering with Self-Assembling Au@Ag@β-Cyclodextrin Bimetal Nanoparticles to Fabricate a Ring-like Arrayed SERS Substrate for Sensitive Recognition of Phthalate Esters Based on a Host−Guest Interaction and the Coffee Ring Effect. *Anal. Methods* **2022**, *14*, 259−268.
(38) Yu, W. W.; White, I. M. Inkjet Printed Surface Enhanced Raman Spectroscopy Array on Cellulose Paper. *Anal. Chem.* **2010**, *82*, 9626−9630.
(39) Chen, R.; Zhang, L.; Li, X.; Ong, L.; Soe, Y. G.; Sinsua, N.; Gras, S. L.; Tabor, R. F.; Wang, X.; Shen, W. Trace Analysis and Chemical Identification on Cellulose Nanofibers-Textured SERS Substrates Using the "Coffee Ring" Effect. *ACS Sens.* **2017**, *2*, 1060−1067.
(40) Huang, Z.; Nagpal, A.; Siddhanta, S.; Barman, I. Leveraging Coffee-Ring Effect on Plasmonic Paper Substrate for Sensitive Analyte Detection Using Raman Spectroscopy. *J. Raman Spectrosc.* **2018**, *49*, 1552−1558.
(41) Law, K.-Y. Definitions for Hydrophilicity, Hydrophobicity, and Superhydrophobicity: Getting the Basics Right. *J. Phys. Chem. Lett.* **2014**, *5*, 686−688.
(42) Wang, W.; Yin, Y.; Tan, Z.; Liu, J. Coffee-Ring Effect-Based Simultaneous SERS Substrate Fabrication and Analyte Enrichment for Trace Analysis. *Nanoscale* **2014**, *6*, 9588−9593.
(43) Nguyen, T. A. H.; Nguyen, A. V. Increased Evaporation Kinetics of Sessile Droplets by Using Nanoparticles. *Langmuir* **2012**, *28*, 16725−16728.
(44) Contreras-Naranjo, J. E.; Aguilar, O. Suppressing Non-Specific Binding of Proteins onto Electrode Surfaces in the Development of Electrochemical Immunosensors. *Biosensors* **2019**, *9*, No. 15.
(45) Sempels, W.; De Dier, R.; Mizuno, H.; Hofkens, J.; Vermant, J. Auto-Production of Biosurfactants Reverses the Coffee Ring Effect in a Bacterial System. *Nat. Commun.* **2013**, *4*, No. 1757.

https://doi.org/10.1021/acsomega.3c03690
ACS Omega 2023, 8, 33745−33754

(46) Abraham, S.; Ha, C.-S.; Batt, C. A.; Kim, I. Synthesis of Stable "Gold Nanoparticle−Polymeric Micelle" Conjugates: A New Class of Star "Molecular Chimera" That Self-Assemble into Linear Arrays of Spherical Micelles. *J. Polym. Sci., Part A: Polym. Chem.* **2007**, *45*, 3570−3579.
(47) Liu, Y.; Guo, R. The Interaction between Casein Micelles and Gold Nanoparticles. *J. Colloid Interface Sci.* **2009**, *332*, 265−269.
(48) Hait, S. K.; Moulik, S. P. Determination of Critical Micelle Concentration (CMC) of Nonionic Surfactants by Donor-Acceptor Interaction with Iodine and Correlation of CMC with Hydrophile-Lipophile Balance and Other Parameters of the Surfactants. *J. Surfactants Deterg.* **2001**, *4*, 303−309.
(49) TWEEN 20 viscous liquid | 9005-64-5. 2021, https://www.sigmaaldrich.com/US/en/product/sial/p1379?context=product (accessed November 16, 2021).
(50) Huang, C. C.; Tseng, W. L. Highly Selective Detection of Histidine Using O-Phthaldialdehyde Derivatization after the Removal of Aminothiols through Tween 20-Capped Gold Nanoparticles. *Analyst* **2009**, *134*, 1699−1705.
(51) Capocefalo, A.; Mammucari, D.; Brasili, F.; Fasolato, C.; Bordi, F.; Postorino, P.; Domenici, F. Exploring the Potentiality of a SERS-Active PH Nano-Biosensor. *Front. Chem.* **2019**, *7*, No. 413.
(52) Efrima, S.; Zeiri, L. Understanding SERS of Bacteria. *J. Raman Spectrosc.* **2009**, *40*, 277−288.
(53) Witkowska, E.; Korsak, D.; Kowalska, A.; Janeczek, A.; Kamińska, A. Strain-Level Typing and Identification of Bacteria − a Novel Approach for SERS Active Plasmonic Nanostructures. *Anal. Bioanal. Chem.* **2018**, *410*, 5019−5031.
(54) Chao, Y.; Zhang, T. Surface-Enhanced Raman Scattering (SERS) Revealing Chemical Variation during Biofilm Formation: From Initial Attachment to Mature Biofilm. *Anal. Bioanal. Chem.* **2012**, *404*, 1465−1475.
(55) De Gelder, J.; De Gussem, K.; Vandenabeele, P.; Moens, L. Reference Database of Raman Spectra of Biological Molecules. *J. Raman Spectrosc.* **2007**, *38*, 1133−1147.
(56) Zong, C.; Xu, M.; Xu, L.-J.; Wei, T.; Ma, X.; Zheng, X.-S.; Hu, R.; Ren, B. Surface-Enhanced Raman Spectroscopy for Bioanalysis: Reliability and Challenges. *Chem. Rev.* **2018**, *118*, 4946−4980.
(57) Liu, T.-T.; Lin, Y.-H.; Hung, C.-S.; Liu, T.-J.; Chen, Y.; Huang, Y.-C.; Tsai, T.-H.; Wang, H.-H.; Wang, D.-W.; Wang, J.-K.; Wang, Y.-L.; Lin, C.-H. A High Speed Detection Platform Based on Surface-Enhanced Raman Scattering for Monitoring Antibiotic-Induced Chemical Changes in Bacteria Cell Wall. *PLoS One* **2009**, *4*, No. e5470.
(58) Zhou, H.; Yang, D.; Ivleva, N. P.; Mircescu, N. E.; Niessner, R.; Haisch, C. SERS Detection of Bacteria in Water by in Situ Coating with Ag Nanoparticles. *Anal. Chem.* **2014**, *86*, 1525−1533.
(59) Pang, Y.; Wan, N.; Shi, L.; Wang, C.; Sun, Z.; Xiao, R.; Wang, S. Dual-Recognition Surface-Enhanced Raman Scattering(SERS)-Biosensor for Pathogenic Bacteria Detection by Using Vancomycin-SERS Tags and Aptamer-Fe3O4@Au. *Anal. Chim. Acta* **2019**, *1077*, 288−296.
(60) Pearson, B.; Wang, P.; Mills, A.; Pang, S.; McLandsborough, L.; He, L. Innovative Sandwich Assay with Dual Optical and SERS Sensing Mechanisms for Bacterial Detection. *Anal. Methods* **2017**, *9*, 4732−4739.
(61) Abràmoff, M. D.; Magalhães, P. J.; Ram, S. J. Image Processing with ImageJ. *Biophotonics Int.* **2004**, *11*, 36−41.
(62) Lieber, C. A.; Mahadevan-Jansen, A. Automated Method for Subtraction of Fluorescence from Biological Raman Spectra. *Appl. Spectrosc.* **2003**, *57*, 1363−1367.
(63) He, S.; Zhang, W.; Liu, L.; Huang, Y.; He, J.; Xie, W.; Wu, P.; Du, C. Baseline Correction for Raman Spectra Using an Improved Asymmetric Least Squares Method. *Anal. Methods* **2014**, *6*, 4402−4407.
(64) *Handbook of Applied Multivariate Statistics and Mathematical Modeling*; Tinsely, H.; Brown, S., Eds.; Academic Press, 2000.
(65) McHugh, M. L. Multiple Comparison Analysis Testing in ANOVA. *Biochem. Med.* **2011**, *21*, 203−209.

https://doi.org/10.1021/acsomega.3c03690
ACS Omega 2023, 8, 33745−33754